A new rapid thermographic method to assess the fatigue limit in GFRP composites

Davide Palumbo, Rosa de Finis, Pompeo Giuseppe Demelio, Umberto Galietti

Composites Part B 103 (2016) 60–67

Contents lists available at ScienceDirect

Composites Part B

journal homepage: www.elsevier.com/locate/compositesb

A new rapid thermographic method to assess the fatigue limit in GFRP composites

Davide Palumbo, Rosa De Finis*, Pompeo Giuseppe Demelio, Umberto Galietti

Department of Mechanics Mathematics and Management (DMMM), Politecnico di Bari, Viale Japigia 182, 70126, Bari, Italy

ARTICLE INFO

Article history:
Received 2 May 2016
Received in revised form
14 July 2016
Accepted 12 August 2016
Available online 15 August 2016

Keywords:
GFRP composites
Thermography
TSA
Fatigue damage
Fatigue limit

ABSTRACT

Conventional procedures and methods used for obtaining the fatigue performance of materials represent a critical aspect of mechanical characterization because of time consuming tests with a high number of specimens. In the last few years, great efforts have been made to develop a number of methods aimed at reducing testing time and, subsequently, the cost of the experimental campaign. In the process, thermographic methods have shown to be a useful tool for the rapid evaluation of fatigue damage and fatigue limit.

This work deals with a new procedure for the evaluation of fatigue limit and the monitoring of damage in GFRP material by means of thermography. Although damage mechanisms in composite materials are difficult to understand, the proposed procedure allows us to obtain a number of parameters providing information relating to the onset of failure phenomena. It is worth noting that the reported procedure provides results in good agreement with those attained by the standard test methods.

1. Introduction

Composite materials are nowadays used to produce large structures in many applications ranging from boating-yachting to aeronautical or aerospace [1]. In this regard, wind turbine blades are made from polymer composites since a highly specific rigidity is required, in addition to strength and good mechanical behaviour [2]. In particular, the fatigue performances imposed by Standards have to be verified by means of experimental campaigns in laboratory on sample specimens or directly on large components. Classical procedures for evaluating the fatigue limit of material involves expensive and time-consuming tests because of the high number of specimens being tested [3].

In recent years, with an aim to reduce testing times and costs of fatigue tests, different techniques and methods have been proposed in order to study the various damage phenomena rapidly and consistently [4–7]. In particular, Infrared Thermography Technique (IRT) represents a reliable support for investigating fatigue damage in metallic and composite materials [8–11]. The great interest in IRT is due to the possibility it provides for the assessment of information about fatigue behaviour by studying the heat sources generated during tests [12–16].

Luong [17] and Risitano [18] proposed a graphical method to assess the fatigue limit of metallic materials by monitoring the superficial temperature of the specimen during an incremental stepwise procedure. The same approach has been employed in Montesano's work [12] for determining the fatigue limit of polymer matrix composites (PMC). In this case, the lifespan curve has been determined by means of IRT and an excellent correlation with the conventional stress-life curve was obtained. Two different approaches (passive and active) have been applied in the work of Steinberger et al. [13]. In particular, a quantitative characterization of damage has been performed by calculation of the loss factor via hysteretic heating.

In another approach, different authors [19,20] use a specific data processing of recorded infrared sequences to investigate the damage phenomena in the material. In this case, the temperature signal is analyzed in the time domain so that the first and the second order harmonics of the signal can be used to describe the nonlinear thermal signal component, due to the thermomechanical coupling phenomena. This approach has been used in the work of Kordatos et al. [21] to study the fatigue behaviour of aluminum grade 1050 H16 and SiC/BMAS ceramic matrix composite cross-ply specimens by combining lock-in thermography (dissipative heat source analysis) and acoustic emission techniques. In this case, as well, IRT provides a good estimation of the material life in the finite life

* Corresponding author.
E-mail address: rosa.definis@poliba.it (R. De Finis).

http://dx.doi.org/10.1016/j.compositesb.2016.08.007
1359-8368/

region.

In other works [22–26], the potential to identify minimal damage by means of Thermoelastic stress Analysis (TSA) has been demonstrated.

Thermoelastic Stress Analysis (TSA) is a non-contact, full field technique that provides stress maps of a component subjected to dynamic loading [22–26]. This technique is based on the thermoelastic effect: a component undergoing dynamic load exhibits a small and reversible temperature change. In adiabatic and linear elastic conditions, these temperature changes are proportional to the first stress invariant. Procedures based on TSA have been developed in the last few years for the damage monitoring of standard specimens and welded joints made of metallic materials (steel, titanium and aluminum) [27,28].

The potential of TSA for analyzing composite materials has been reported in the works of Emery et al. [14] and Fruehmann et al. [15]. In particular, the first investigates various polymer-matrix-composites with different laminate types, while the second highlights the possibility of using the phase signal for evaluation of fatigue damage, even at low stress.

In this work, a novel procedure for processing thermographic data is shown which can illustrate the fatigue behaviour of GFRP composites and provides a rapid evaluation of the fatigue limit of material. The strong point of the proposed method is the possibility to obtain with a single analysis of thermographic data, information about dissipative heat sources and thermoelastic heat sources. This analysis has been applied for several fatigue tests on five standard specimens made of GFRP composite material. Each test has been monitored at regular intervals with a cooled infrared camera. Finally, conventional fatigue tests were also performed in order to offer a comparison with the proposed thermal procedure.

2. Theory

Generally, during fatigue tests, two thermal effects are generated: thermoelastic heat sources and intrinsic dissipations. The first represents the well-known thermoelastic coupling while, intrinsic dissipation is thermodynamically irreversible and is due to various factors including the viscoelastic nature of the matrix material, matrix cracking, fibre fracture, and interface cracking/friction [12].

Under the hypotheses of adiabatic conditions, temperature changes ΔT_{el} for orthotropic materials are related to changes in the stresses in the principal material directions by the following expression:

$$\Delta T_{el} = -\frac{T_0}{\rho C_p}(\alpha_1 \Delta\sigma_1 + \alpha_2 \Delta\sigma_2) \tag{1}$$

where α_1 and α_2 are the coefficients of linear thermal expansion relative to the principal axes, C_p is the specific heat at constant pressure, ρ is the density, T_0 is the absolute temperature and $\Delta\sigma_1$and $\Delta\sigma_2$ are the principal stresses.

The adopted acquisition systems of TSA, usually provide a non-radiometrically calibrated S signal proportional to the peak-to-peak variation in temperature during the peak-to-peak variation of the sum of principal stress. S is usually presented as a vector, where modulus is proportional to the change in temperature due to the thermoelastic effect and the phase φ means the angular shift between the thermoelastic and the reference signal [14]. In this case, the following equation can be used:

$$A^*S = (\alpha_1 \Delta\sigma_1 + \alpha_2 \Delta\sigma_2) \tag{2}$$

where A^* is a calibration constant.

The signal S can be expressed in time domain as follows:

$$s_{th} = \frac{S}{2}\sin(\omega t + \pi + \phi) \tag{3}$$

where s is the non-calibrated thermoelastic signal, ω is the angular velocity and φ is the phase angle between temperature and loading signal. This angle depends on a number of parameters such as, for example, thickness of the painting or the grips of the loading machine. Whilst phase can slightly change through the area analyzed due to non-perfect homogeneity of the surface conditions, it remains locally constant in presence of linear elastic behaviour of material and adiabatic conditions. In the event of damage occurring, non-linearity of thermoelastic signal and phase variations can be observed [15].

As shown in Equation (3), the thermoelastic signal varies at the same frequency as the loading during the test.

It was demonstrated that the intrinsic dissipations occurred at twice the frequency of mechanical loading and are two orders lower than the thermoelastic type [19,21]. The dissipative terms are irreversible sources unlike the thermoelastic type, causing the increase in the mean temperature of the specimen.

In effect, in presence of damage, a typical three-stage trend is reported in surface temperature measurement [16]; firstly, there is a mean temperature increase, secondly, it reaches an equilibrium value due to balancing in elastic dissipative sources and heat exchange effect [29].

Following the temperature plateau achieved, in the eventuality of failure occurring at a certain loading step, temperature will increase abruptly, as reported in Ref. [16].

Considering dissipative heat sources, the related thermal signal can be modelled by means of the following equation:

$$s_d = S2\,\sin(2\omega t) \tag{4}$$

where s_d is the non-calibrated thermographic signal correlated with irreversible sources and $S2$ is the amplitude signal of thermal sources.

3. Experimental set-up

Twelve specimens were extracted from a laminate panel made of an epoxy-type resin reinforced with two internal layers of cross-plied quasi-isotropic glass fiber $+45°/0°/-45°/90°$ and two external layers of unidirectional fiber of the $0°/90°$ type. The fiber volume fraction was 63% while the matrix volume fraction was 37%. The overall density of composite was 175 g/cm^3 and the resin density was 110 g/cm^3.

The dimensions of specimens were fixed according to Standard ASTM D 3039 which were 25 mm wide, 250 mm long and 2.5 mm thick. All the specimens were tested on an MTS (model 370, 100 kN capacity) servo-hydraulic machine.

The specimens were firstly, statically tested, to assess mechanical ultimate tensile strength. The tests provided 440 MPa. Conventional procedure was applied to test seven of the produced

Table 1
Stresses and number of cycles to failure obtained on seven specimens.

Step	σ max [MPa]	Number of cycles
1	380	400
2	270	2630
3	240	13,521
4	200	52,434
5	175	120,540
6	150	351,588
7	138.5	1,189,803

twelve specimens, providing the S-N curve and estimate of the fatigue limit. In Table 1, the maximum stress applied adopting a stress ratio of 0.1 and a loading frequency of 7 Hz is shown.

The same fatigue test parameters were used for the thermographic tests on the five leftover specimens. In this case, as shown in Table 2, a loading stepped procedure was performed starting with nominal stress amplitude ($\Delta\sigma/2$) of 30 MPa. At the end of each step (about 10,000 cycles of loading machine), the applied load was increased according to the values shown in Table 2.

The adopted experimental set-up for thermographic tests is shown in Fig. 1.

An IR cooled In-Sb detector FLIR X6540 SC (640X512 pixel matrix array, thermal sensitivity NETD < 30 mK) has been used both to collect the thermal data and for the monitoring of superficial temperature of specimens.

Referring to the fixed stress level, three thermal sequences were acquired respectively at 2000, 6000 and 8000 cycles, to investigate the damage within each loading step. These sequences in the paper will be indicated as Substep 1 (2000 cycles), Substep 2 (6000 cycles) and Substep 3 (8000 cycles).

The adopted frame rate was 100 Hz. Each acquisition lasts 10 s, therefore 1000 frames were recorded. Thermal sequences were analyzed by Matlab® software.

4. Methods and data analysis

A mathematical algorithm has been used to extract information pixel by pixel regarding parameters related to the surface temperature of the specimen, the signal amplitude, the phase of the thermoelastic signal and the amplitude of the second Fourier harmonic component associated with the intrinsic dissipations. In particular, a suitable thermographic signal model was used to study the thermal signal S_m evolution (not radiometrically calibrated) in the time domain, as indicated in Equation (5):

$$S_m(t) = S_0 + at + S1\,\sin(\omega t + \phi) + S2\,\sin(2\omega t) \quad (5)$$

where the term $S_0 + at$ represents the increase in mean temperature during cyclic mechanical loading in terms of radiometric signal, ω is angular frequency of the mechanical imposed load, $S1$and φ are respectively related to the amplitude and the phase of the first harmonic component of the Fourier series while $S2$ represents the amplitude of the second Fourier harmonic component. Therefore, the term $S1$ corresponds to the signal variation related to thermoelastic effect and $S2$ is proportional to the amplitude of intrinsic dissipation.

Equation (5) was integrated in the algorithm of IRTA® software providing images in the form of data matrix for each constant parameter. The phase φ of thermoelastic signal has not been taken into account in this paper since it will be shown in a further work.

The procedure for the processing of thermographic data was applied for each loading step and sub-step and provides:

- The acquisition of the thermographic sequence. About one thousand frames were acquired for each sequence.
- Assessing of the three thermal signals: S_0, $S1$and $S2$ pixel by pixel (IRTA® software).
- Application of a Gaussian 2D-smoothing on IRTA® data matrix for the purposes of noise reduction. In this regard, the Gaussian kernel provides a gentler smoothing and preserves edges better than a similarly sized mean filter.
- Reduction of data matrix (area of analysis) to refer the analysis only to the area of gauge length. In this case, the area of analysis was the same for S_0, $S_1$and S_2 (A1 area, Fig. 2), and includes 405x49 pixels (mm/pixel = 0.4).

For signal S_0 (radiometric temperature signal), the processing steps are:

- Subtracting the environmental temperature influence on temperature signal S_0 achieved during each step and sub-step (ΔS_0), which is required in order to obtain a good estimation of the temperature changes which are due to material damage. Environmental temperature signal has been measured by using a dummy specimen (A2 area in Fig. 2).
- Evaluation of the 98th value of percentile to avoid outliers in temperature signal measurements (ΔS_{0_98perc}) in the considered data matrix (A1 area). As stated by Refs. [30], since the energy of damage is proportional to the dissipated energy as heat per cycle, in order to closely follow the dissipation phenomena, 98th percentile temperature value is chosen as a guideline.

For signal $S1$ (thermoelastic signal), the analysis involves:

Table 2
Number of loading steps and correspondent applied stresses.

N	Δσ/2 [MPa]	σ min [MPa]	σ max [MPa]	σ mean [MPa]
1	30	4	44	24
2	35	7	67	37
3	40	8	78	43
4	45	9	89	49
5	50	10	100	55
6	55	11	111	61
7	60	12	122	67
8	65	13	133	73
9	70	14	144	79
10	75	16	156	86
11	80	17	167	92
12	85	18	178	98
13	90	20	200	110
14	100	22	222	122

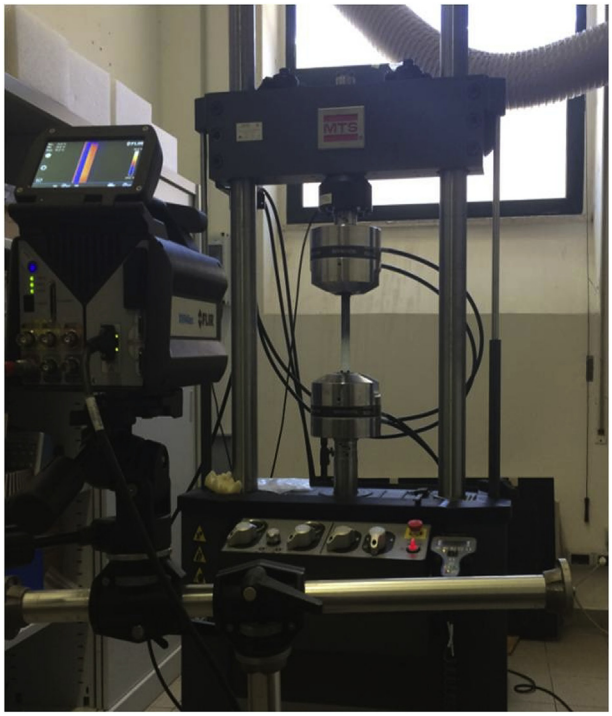

Fig. 1. Experimental set-up adopted for thermographic tests.

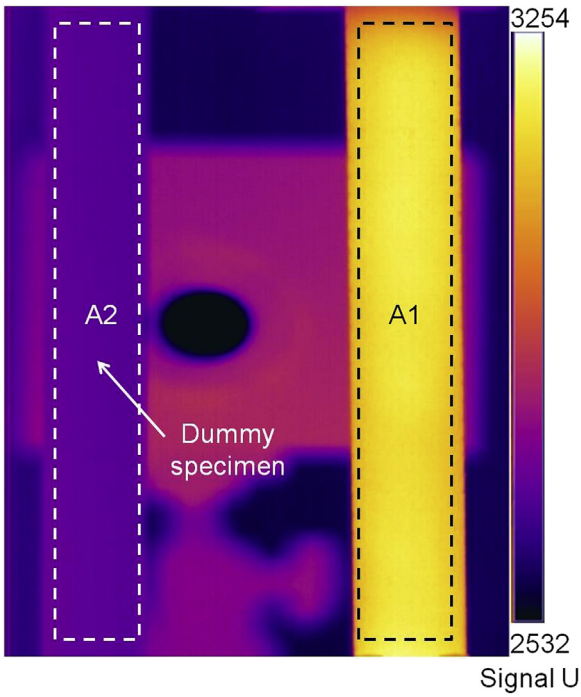

Fig. 2. Area considered for the analysis (A1) and for evaluating of environmental temperature signal (A2, dummy specimen).

- Subtracting a thermoelastic amplitude data matrix of the first loading step when no damage occurred to provide a reference condition between damaged and undamaged situations. In this way, the thermoelastic variations are related to an undamaged reference condition (ΔS_1).
- Normalizing the thermoelastic data matrix with respect to the stress amplitude $\Delta\sigma$ in order to detect the thermoelastic signal variation associated with damage ($S1_{norm} = \Delta S_1/\Delta\sigma$).
- Evaluation of the maximum and the minimum values of the thermoelastic signal ($\Delta S_1/\Delta\sigma$) in order to assess the $\Delta S1_{norm} = S1_{norm\_max} - S1_{norm\_min}$ from the data matrix. In order to avoid isolated bad pixels due for example, to "dead pixels", values of 98th and 2nd percentile have been used in this paper in place of $S1_{norm\_max}$ and $S1_{norm\_min}$ ($\Delta S1_{norm\_98\text{-}2perc}$).

The processing of signal component *S2* (radiometric thermographic signal correlated to the intrinsic dissipations) refers to the:

- assessment of 98th percentile value of the *S2* signal (S_{2_98perc}).The choice of 98th percentile value is held up by the fact that signal variations are so low when compared to the other parameters, thus, the end of excluding the influence of isolated bad pixels in the analysis is pursued.

The procedure is shown in Fig. 3 in a graphic flow-chart form.

5. Results and discussions

In Fig. 4, the convectional curve S-N obtained is shown together with the data of Table 1 (seven of the specimens tested) which allows for the estimation of the fatigue limit of material for a conventional number of cycles. To derive an interval estimation of 'future' observation, it would be appropriate to include in the graph in Fig. 4, a 90% survival probability (prediction straight lines) using a confidence interval of 95%, (dashed lines in Fig. 4).

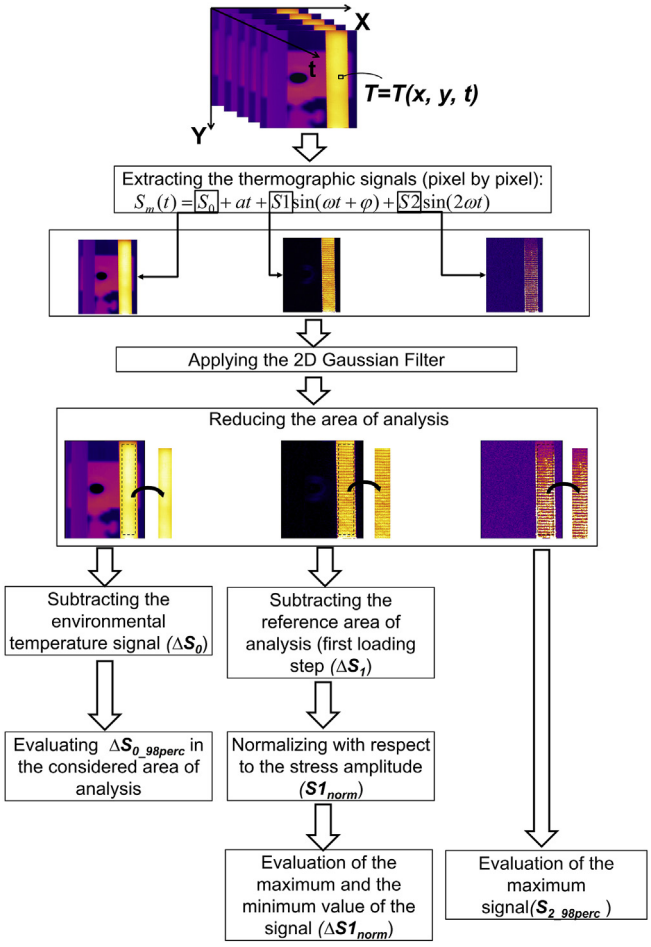

Fig. 3. Flow chart of the proposed procedure.

Considering a number of 2×10^6 cycles as lifetime reference within High Cycle Fatigue as suggested by Standard Test Method [31], a value of 127.4 MPa is extracted by data series, representing the fatigue limit in terms of σ_{max} and of 56.12 MPa in terms of stress amplitude ($\Delta\sigma/2$).

Fig. 5 shows the evolution of the temperature signal expressed as radiometric signal (ΔS_0) for Specimen 1 and for four different loading conditions (Substep 3). The depicted curve in Fig. 5 refers to the mean temperature trend during the stepwise procedure and has been already discussed by several authors [16–18,30]. A uniform increase of the signal is obtained in the whole gauge area and even in the last loading step (90 MPa) local differences of signal in correspondence to damage, are observed.

In the same way, in Fig. 6, the maps of thermoelastic signal (Specimen 1, Substep 3) are reported.

Considering the reference stress condition of 30 MPa, thermoelastic signal experiences positive and negative value variations. As already demonstrated in other works [14,15], TSA allows for location of the damaged areas of material and in particular, the thermoelastic signal variations are related to the redistribution of the stresses caused by stiffness degradation due to damage [15].

As confirmed by other authors [15], by analyzing stress maps, mechanical behaviour of fibers and matrix is indeed assessed.

In Fig. 7, the maps of the thermal signal at twice the loading frequency are shown (Specimen 1, Sub step 3). In addition, in this case, a significant increase of the signal is obtained as the applied stress increases.

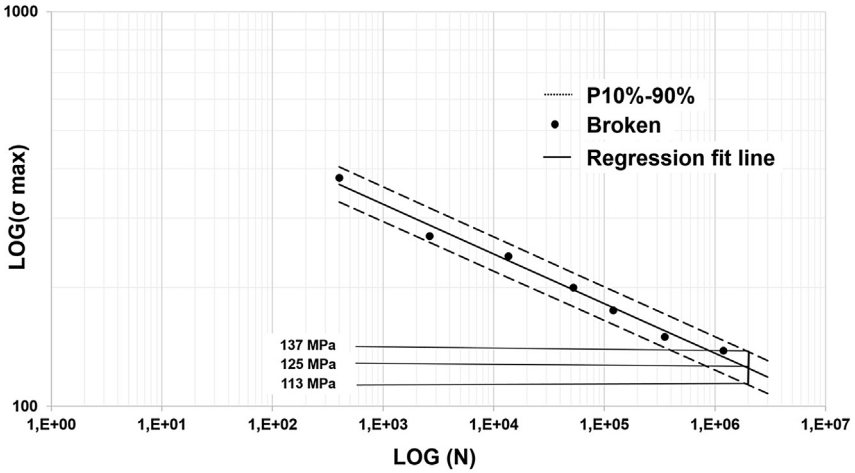

Fig. 4. Conventional S-N curve and estimation of the fatigue limit in correspondence with a run-out limit of 2×10^6 cycles.

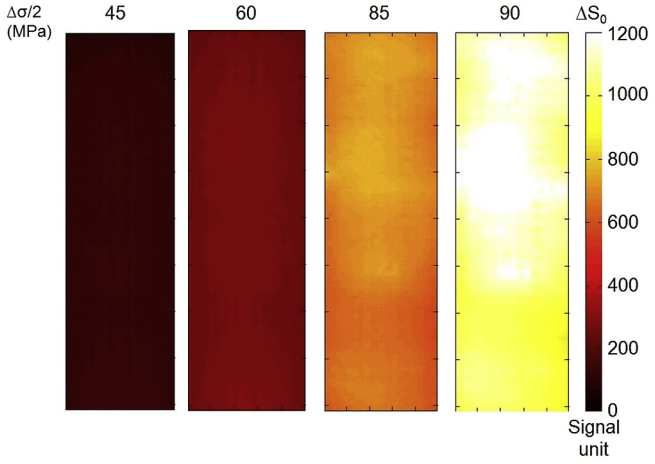

Fig. 5. Maps of the radiometric signal obtained for four different loading steps, (Specimen 1, Sub-step 3).

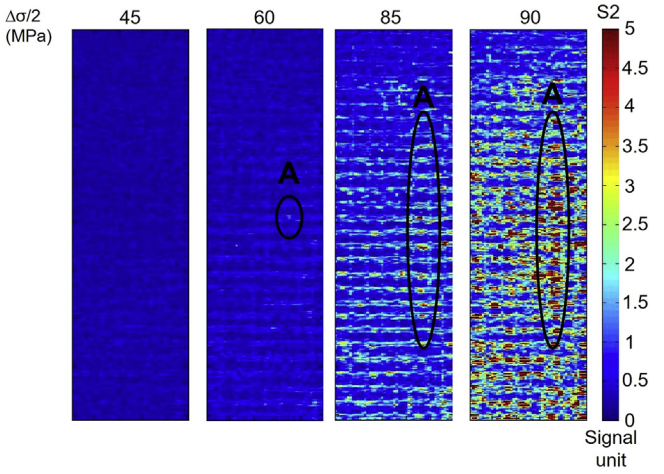

Fig. 7. Maps of the thermographic signal at the twice the loading frequency obtained for four different loading steps, (Specimen 1, Sub-step3).

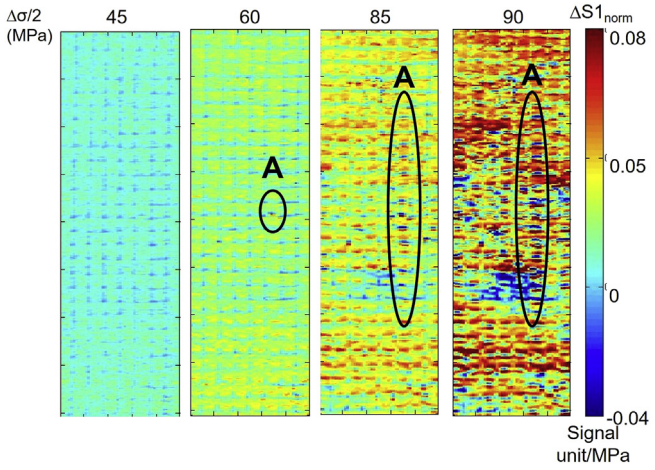

Fig. 6. Maps of the thermoelastic signal obtained for four different loading steps, (Specimen 1, Sub-step 3).

As demonstrated by parameter maps at a fixed stress level of 60 MPa, the failure appears on the right side of the gauge length as depicted in Figs. 6 and 7 (Area A, crack initiation at 60 MPa). At 90 MPa, the occurrence of cracks hits most of the gauge length.

All maps seem to provide different and complementary information about the type of damage to material. In this regard, further works and other experimental techniques are necessary to relate the different damage mechanisms to the proposed thermographic signal procedure.

The trend of the signals evaluated with the proposed algorithm is shown in Fig. 8 as a function of the amplitude stress for each sub-step. In particular, the radiometric temperature signal increases for each loading step due to the viscoelastic nature of the matrix material until a significant increase is verified in correspondence with the presence of the damage mechanisms, while thermoelastic ($S1$) and double frequency signal ($S2$) show significant variations only for stress values above 60 MPa.

Interesting considerations can be made by observing signal behaviour in correspondence with each sub-step, Fig. 8. In fact, no appreciable signal differences are present among the three sub-steps excluding the last loading step coincident with the failure of the specimen.

The procedure described in the work of De Finis et al. [16] has been used for evaluating the fatigue limit for each measured signal ($\Delta S0_{\_98perc}$, $\Delta S1_{norm\_98\text{-}2perc}$ and $S2_{98\_perc}$). For each specimen and for

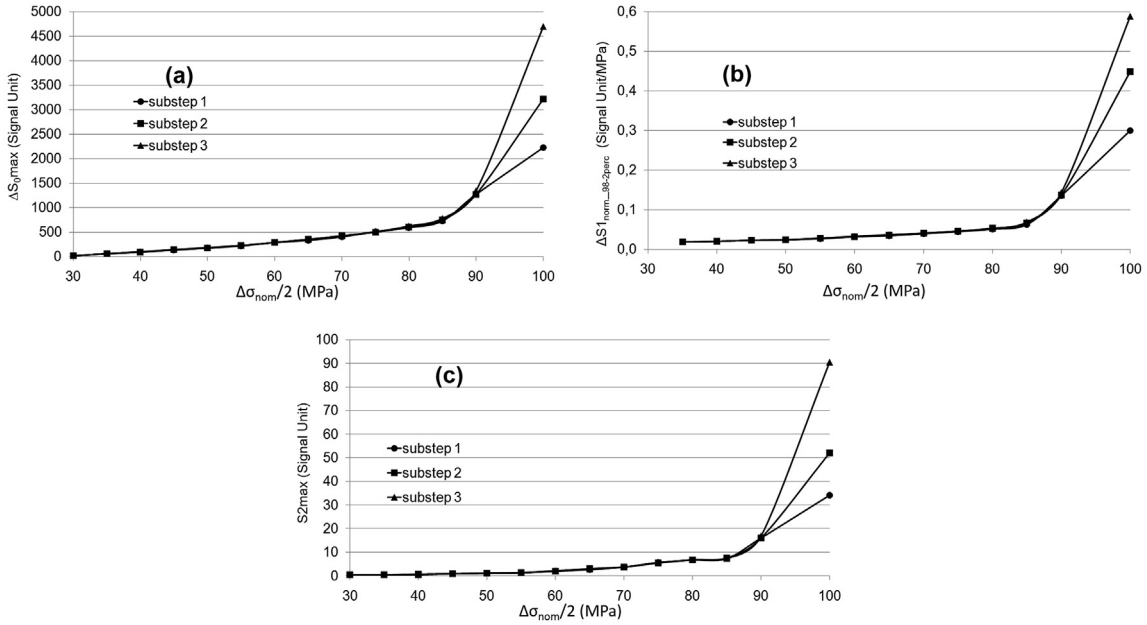

Fig. 8. Thermographic signals obtained with proposed procedure as function of the amplitude stress for Specimen 1: comparison among the three sub-steps for the parameter (a)ΔS_0, (b) ΔS_1 (c)S_2.

each sub-step, the adopted procedure consists of:

1 Linear regression analysis of the first 4 data couples (P; $\Delta\sigma/2$) and evaluation of the best fit line ($y = mx + q$). P represents the generic thermographic signal.
2 Evaluation of residuals of P (P_r) for each loading step.
3 Evaluation of standard deviation (σP_r) and mean (μ) of residuals (P_r) of the first 4 data for each test.
4 Evaluation of the threshold value as Pth = $\mu+6 \times \sigma$P_r
5 Evaluation of the first loading step (of P_r data) for which the condition: (P_r) N > Pth is verified (where N is the number of the loading step). The first loading step exceeding the condition is considered the estimation of fatigue limit.

Fig. 9(a, c) graphically illustrates the above procedure for Specimen 1 at Substep 3. In particular, the residuals are plotted versus the stress amplitude and the dotted line represents the threshold value adopted for the estimation of the fatigue limit. By using other methods it may be difficult to detect this point. The graphical approach [17,18], which involves separation of the data series for the assessment of the breakpoint, is not objective, and deduction and identification are hindered due to the noise affecting thermal measurements.

In Table 3, the results (fatigue limits in terms of stress semi-amplitudes) for each parameter (ΔS_{0_98perc}, $\Delta S1_{norm\_98\text{-}2perc}$ and $S2_{\_98perc}$) at each sub-step are reported for five tested specimens.

As shown in Table 3, referring to a single test, the results show good reproducibility and thus, the reliability of the technique is demonstrated.

This aspect is confirmed by Table 4 in which overall results of five tests are compared with the standard test method. The results of thermal methods fit well with the S-N value reference as endorsed by the small standard deviation. In particular, referring to the analysis of three parameters the closest one to the reference value (56.12 MPa) is the $S2_{\_98perc}$ parameter (~58 MPa), although the others provide a good estimation of fatigue limit.

As already shown in Fig. 8(a–c), no difference exists among sub-steps and the adopted procedure for evaluating the fatigue limit provides the same value for each sub-step. Moreover, the considered thermographic parameters for low stress values seem independent from the number of cycles at which the thermographic sequence was acquired. This means that an estimation of the fatigue limit could be obtained with the proposed procedure very rapidly since the thermographic data can be acquired at any time during the tests, whilst for the traditional procedure it is necessary to achieve steady state conditions before acquisition.

Results obtained with thermography techniques are in good agreement with the fatigue limit obtained in the conventional manner by considering a run-out limit of 2×10^6 cycles.

6. Conclusions

In this work, a novel application of Infrared thermography has been discussed capable of evaluating the fatigue limit of GFRP composite materials in a rapid way and damage behaviour. The applied processing procedure allows for assessing by a single test, several index adopted to study fatigue by different perspectives.

The innovation with respect previous works refers to the possibility of a fully/in-depth understanding of damage by comparing different parameter in a synergetic way. To do this, the uncalibrated thermal signal was processed in the time domain, to study the increasing of the mean temperature of the specimen, the thermoelastic source and the intrinsic dissipations. The results show good reproducibility within a single loading level (for different thermal acquisitions) and between tests.

Referring to the test and processing procedures it is worth noting the rapidity of the approach for assessing fatigue limit and for detecting the onset of damage. Moreover, since the method for fatigue limit estimation involves fixing a threshold value, it may be unnecessary bring specimens to failure.

The adopted statistical method has been validated for metallic materials, and results are in good agreement with those obtained by the conventional S-N curve.

The potential of this approach could be exploited in the field of non-destructive controls as well as for the monitoring of large and operating complex components undergoing actual loading conditions.

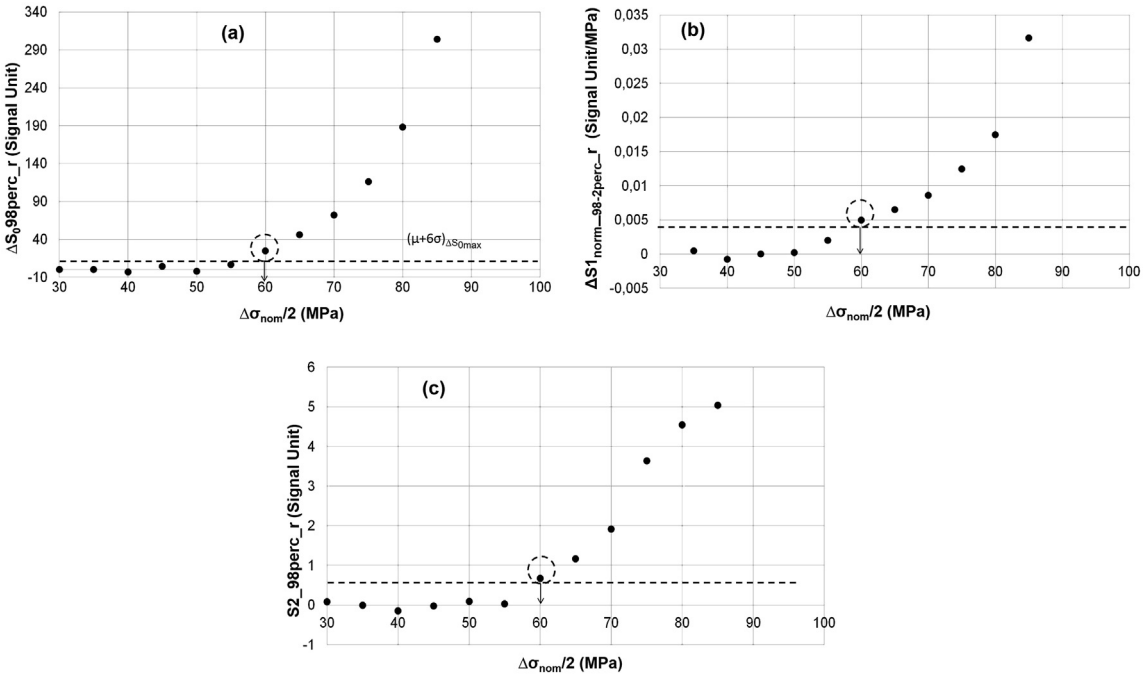

Fig. 9. Estimation of the fatigue limit with method [16], (Specimen 1, Sub-step 3): comparison among residual of the three parameters (a)ΔS_0, (b)ΔS_1 (c)S_2.

Table 3
Comparison between overall results in sub-step, accomplished by adopting the thermographic technique.

N specimen	Loading sub-step	ΔS_{0_98perc} (MPa)	$\Delta S1_{norm\_98\text{-}2perc}$ (MPa)	$S2_{\_98perc}$ (MPa)
1	1	60.00	60.00	65.00
	2	60.00	60.00	60.00
	3	60.00	60.00	60.00
	Average	60.00	60.00	61.67
2	1	60.00	60.00	60.00
	2	60.00	60.00	60.00
	3	60.00	65.00	60.00
	Average	60.00	61.67	60.00
3	1	60.00	65.00	55.00
	2	60.00	70.00	55.00
	3	60.00	65.00	50.00
	Average	60.00	66.67	53.33
4	1	70.00	55.00	55.00
	2	65.00	55.00	70.00
	3	65.00	70.00	55.00
	Average	66.67	60.00	60.00
5	1	60.00	65.00	55.00
	2	55.00	65.00	50.00
	3	55.00	65.00	55.00
	Average	56.67	65.00	53.33

Table 4
Comparison between overall results accomplished by adopting the thermographic technique and conventional fatigue tests.

N specimen	ΔS_{0_98perc} (MPa)	$\Delta S1_{norm\_98\text{-}2perc}$ (MPa)	$S2_{\_98perc}$ (MPa)	S-N curve (2×10^6 cycles)
1	60.00	60.00	61.67	$\Delta\sigma/2 = 56.12$ MPa
2	60.00	61.67	60.00	
3	60.00	66.67	53.33	
4	66.67	60.00	60.00	
5	56.67	65.00	53.33	
Average	**60.67**	**62.67**	**57.67**	
Standard deviation	**3.65**	**3.03**	**4.01**	

References

[1] Bannister MK. Development and application of advanced textile composites. Proc Inst Mech Eng Part L J Mater Des Appl 2004;218:253–60.
[2] Palumbo D, Tamborrino R, Galietti U, Aversa P, Tatì A, Luprano VAM. Ultrasonic analysis and lock-in thermography for debonding evaluation of composite adhesive joints. NDT E Int 2016;78:1–9.
[3] Harris B. Fatigue in composites. Cambridge: Woolhead Publishing Ltd; 2003.
[4] Munoz V, Valès B, Perrin M, Pastor ML, Welemane H, Cantarel A. Damage detection in CFRP by coupling acoustic emission and infrared thermography. Compos Part B 2016;85:68–75.
[5] Goidescu C, Welemane H, Garnier C, Fazzini M, Brault R, Péronnet E, et al. Damage investigation in CFRP composites using full-field measurement technique: combination of digital image stereo-correlation, infrared thermography and X-ray tomography. Compos Part B 2013;48:95–105.
[6] Naderi M, Kahirdeh A, Khonsari MM. Dissipated thermal energy and damage evolution of glass/epoxy using infrared thermography and acoustic emission. Compos Part B 2012;43:1613–20.
[7] Kordatos EZ, Aggelis DG, Matikas TE. Monitoring mechanical damage in structural materials using complimentary NDE techniques based on thermography and acoustic emission. Compos Part B 2012;43:2676–86.
[8] Palumbo D, Ancona D, Galietti U. Quantitative damage evaluation of composite materials with microwave thermographic technique: feasibility and new data analysis. Meccanica 2015;50:443–59.
[9] Palumbo D, Galietti U. Damage investigation in composite materials by means of new thermal data processing procedures. Strain 2016;52:276–85.
[10] U. Galietti, R. Dimitri, D. Palumbo, P. Rubino, Thermal analysis and mechanical characterization of GFRP joints. In: 15th European conference on composite materials: composites at Venice, ECCM 2012, Venice, Italy, 24–28, June, 2012.
[11] Tamborrino R, Palumbo D, Galietti U, Aversa P, Chiozzi S, Luprano VAM. Assessment of the effect of defects on mechanical properties of adhesive bonded joints by using non destructive methods. Compos Part B 2016;91:337–45.
[12] Montesano J, Fawaz Z, Bougherara H. Use of infrared thermography to investigate the fatigue behaviour of a carbon fibre reinforced polymer composite. Compos Struct 2013;97:76–83.
[13] Steinberger R, ValadasLeitão TI, Ladstätter E, Pinter G, Billinger W, Lang RW. Infrared thermographic techniques for non-destructive damage characterization of carbon fibre reinforced polymers during tensile fatigue testing. Int J Fatigue 2006;28:1340–7.
[14] Emery TR, Dulieu-Barton JK. Thermoelastic stress analysis of the damage mechanisms in composite materials. Compos Part A 2010;41:1729–42.
[15] Fruehmann RK, Dulieu-Barton JM, Quinn S. Assessment of the fatigue damage evolution in woven composite materials using infra-red techniques. Compos Sci Technol 2010;70:937–46.
[16] De Finis R, Palumbo D, Ancona F, Galietti U. Fatigue limit evaluation of various martensitic stainless steels with new robust thermographic data analysis. Int J Fatigue 2015;74:88–96.
[17] M.P. Luong, Infrared observation of thermomechanical couplings in solids, Thermosense XXIV conference, part of SPIE′s aerosense 1-Orlando (Florida), 5 April, 2002.
[18] La Rosa G, Risitano A. Thermographic methodology for the rapid determination of the fatigue limit of materials and mechanical components. Int J Fatigue 2000;22:65–73.
[19] Krapez JK, Pacou D, Gardette G. Lock-in thermography and fatigue limit of metals. Quant Infrared Thermogr J 2000;6:277–82.
[20] Ummenhofer T, Medgenberg J. On the use of infrared thermography for the analysis of fatigue damage processes in welded joints. Int J Fatigue 2009;31:130–7.
[21] Kordatos EZ, Dassios KG, Aggelis DG, Matikas TE. Rapid evaluation of the fatigue limit in composites using infrared lock-in thermography and acoustic emission. Mech Res Commun 2013;54:14–20.
[22] Harwood N, Cummings W. Thermoelastic stress analysis. New York: National Engineering Laboratory; Adam Hilger; 1991.
[23] Pittaresi G, Patterson EA. A review of the general theory of thermoelastic stress analysis. J Strain Anal 1999;35:35–9.
[24] Pitarresi G, Galietti U. A quantitative analysis of the thermoelastic effect in CFRP composite materials. Strain 2010;46:446–59.
[25] Wang WJ, Dulieu-Barton JM, Li Q. Assessment of non-adiabatic behaviour in thermoelastic stress analysis of small scale components. Exp Mech 2010;50:449–61.
[26] Palumbo D, Galietti U. Data correction for thermoelastic stress analysis on titanium components. Exp Mech 2016;56:451–62.
[27] Palumbo D, Galietti U. Characterization of steel welded joints by infrared thermographic methods. Quant Infrared Thermogr J 2014;11(1):29–42.
[28] Galietti U, Palumbo D. Application of thermal methods for characterization of steel welded joints. EPJ Web Conf 2010;6:38012.
[29] Maquin F, Pierron F. Heat dissipation measurements in low stress cyclic loading of metallic materials: from internal friction to micro-plasticity. Mech Mater 2009;41:928–42.
[30] Fargione G, Geraci A, La Rosa G, Risitano A. Rapid determination of the fatigue curve by the thermographic method. Int J Fatigue 2002;24:11–9.
[31] Standard test method for tension-tension fatigue of polymer matrix composite materials D3479M-96.